UNIVERSIDADE ESTADUAL PAULISTA "JÚLIO DE MESQUITA FILHO"
CAMPUS DE ILHA SOLTEIRA

ALISSON BALDISSERA

ON THE ORIGIN OF THE HIGH OSCILLATORY SHEAR INDEX IN A PATIENT-SPECIFIC INTRACRANIAL ANEURYSM

Ilha Solteira - SP
2025

ALISSON BALDISSERA

ON THE ORIGIN OF THE HIGH OSCILLATORY SHEAR INDEX IN A PATIENT-SPECIFIC INTRACRANIAL ANEURYSM

Trabalho de Graduação apresentado à Universidade Estadual Paulista (UNESP), Faculdade de Engenharia de Ilha Solteira, para obtenção do título de Bacharel em Engenharia Mecânica.

Orientador(a): Prof. Dr. José Luiz Gasche

Coorientador(a): Prof. Dr. Iago Lessa de Oliveira

Ilha Solteira - SP

2025

COBEM 2025
28TH INTERNATIONAL CONGRESS OF MECHANICAL ENGINEERING

ABCM
Brazilian Society of Mechanical Sciences and Engineering
28th ABCM International Congress of Mechanical Engineering
November 09-14, 2025, Curitiba-PR, Brazil

COB-2025-1516
ON THE ORIGIN OF THE HIGH OSCILLATORY SHEAR INDEX IN A PATIENT-SPECIFIC INTRACRANIAL ANEURYSM

Alisson Baldissera
São Paulo State University (UNESP), School of Engineering, Ilha Solteira. Ave. Brasil, 56; Centro - 15385-007 - Ilha Solteira / SP
alisson.baldissera@unesp.br

Iago Lessa de Oliveira
São Paulo State University (UNESP), School of Engineering, Bauru. Ave. Eng. Luiz Edmundo C. Coube, 14-01; Vargem Limpa - 17033-360 - Bauru / SP
iago.oliveira@unesp.br

Carlos Eduardo Baccin
Neuronterventional Radiologist, Hospital Beneficência Portuguesa of São Paulo. St. Maestro Cardim, 637; Bela Vista - 01323-001 - São Paulo / SP
cebaccin@gmail.com

José Luiz Gasche
São Paulo State University (UNESP), School of Engineering, Ilha Solteira. Ave. Brasil, 56; Centro - 15385-007 - Ilha Solteira / SP
jose.gasche@unesp.br

Abstract. *Aneurysms are dilated regions in arteries walls. Intracranial aneurysms (IAs) are commonly found in a region known as Circle of Willis. The prior risk related to the rupture of an IA is the subarachnoid hemorrhage, that leads to high fatality and morbidity rate, reaching a rate of fatal cases around 50% of the cases. There are two main techniques for the treatment of IAs: surgical intervention and endovascular treatment. Both are implemented to block the blood flow into the aneurysm sac. Although the surgical intervention leads to longer postoperative disabilities and carries some risks related to the craniotomy and the impossibility of clipping some aneurysm geometries, the endovascular treatment has a higher rate of recanalization than the former method depending on the technique used according to the aneurysm location, size and neck measurement. With the advancement of Computation Fluid Dynamics (CFD) methodologies accompanied by the increasing imaging diagnostic techniques quality, a complete mapping of the geometry of a patient-specific cerebral aneurysm is possible. In this context, the aim of this study is to identify the origin of high oscillatory shear index (OSI) regions in the aneurysm surface to provide medical guidance to indicate the most appropriate treatment for a patient-specific. In this way, a portion of the basilar artery that harbors an IA related to the left superior cerebellar artery (SCA) was used as geometry in a CFD study to obtain the velocity, wall shear stress (WSS) and OSI fields, and correlate them to explain the origin of high OSI regions on the aneurysm surface. The results point out that the high OSI values inside the aneurysm sac are caused by the circulation of the flow induced by the shear layer instability at the aneurysm sac opening.*

Keywords: *intracranial aneurysms, wall shear stress, oscillatory shear index, Computational Fluid Dynamics, Finite Volume Method*

1. INTRODUCTION

Aneurysms are abnormally dilatations in arteries walls. They can occur in the walls of any artery of the human vascular system, mostly found in the abdominal aorta and in arteries that reach the brain. Around 3% of the global population carry a cerebral aneurysm (Vlak *et al.*, 2011). The risk related to the rupture of an intracranial aneurysm (IA) is the hemorrhage to the subarachnoid region, which consists of a portion of the human brain located between the pia-mater and the arachnoid layer of the tissues that cover the brain. The subarachnoid hemorrhage (SAH) is a type of stroke with a high fatality and morbidity rate (Etminan *et al.*, 2019), reaching a fatal cases rate of around 50% after hemorrhage occurrence (Van Gijn *et al.*, 2007). Although it may also be the result from a wide range of causes, SAH stems from the rupture of IAs in 85% of cases (Van Gijn and Rinkel, 2001).

Commonly, cerebral aneurysms occur at the base of the brain in a region known as Circle of Willis (Appanaboyina *et al.*, 2009), that consists of an interconnected structure responsible for supplying blood flow between the anterior and posterior brain arterial systems. Cerebral aneurysms require more attention in treatment and generally do not indicate symptoms before the rupture. In turn, the aneurysm initiation, growth and rupture processes are unfortunately not totally

understood. The mechanisms that cover the aneurysm development are intimately related to intracranial environment, mechanobiology, wall biomechanics and hemodynamics (Sforza *et al.*, 2009). In terms of hemodynamics, studies point that some physical parameters of the flow contribute to the development of cerebral aneurysms, such as wall shear stress (WSS) and oscillatory shear index (OSI). Both high and low values of these variables can indicate a process of growth and rupture of an aneurysm (Meng *et al.*, 2014).

Two main techniques are available for the treatment of this vascular disorder: surgical intervention and endovascular treatment. The former is mainly associated with surgical clipping, which involves placing a metal clip at the neck of the aneurysm to block blood flow into it. The latter is a less invasive technique involving the placement of platinum coils within the dome of the aneurysm with the same objective as the former. Typically, stents – expandable metal meshes – are implanted in the vessel to keep the coils inside the aneurysm dome (Appanaboyina *et al.*, 2009) and improve its occlusion with lower rates of recanalization in large neck aneurysms. Since postoperative disabilities are more frequent in patients undergoing surgical interventions compared to those undergoing endovascular treatments, mainly in the posterior circulation IAs, in which studies point out that there is a superiority of coiling over clipping in terms of permanent neurologic deficit (Tsianaka *et al.*, 2019), and due to the disadvantages associated with aneurysm clipping – such as the high risks inherent to craniotomy and the impossibility of clipping certain aneurysms due to their location and shape – in many cases it is necessary to assess the possibility of endovascular treatment. However, this technique also carries its risks. There are cases of secondary aneurysm formation due to coil compaction (Appanaboyina *et al.*, 2009) and the development of adverse hemodynamic conditions due to stent placement (Kim *et al.*, 2007) have been reported. Therefore, it would be interesting to develop a non-invasive methodology to help predicting aneurysm rupture and to provide medical guidance to indicate the most appropriate treatment for a specific patient.

In this regard, Computational Fluid Dynamics (CFD) methodologies have been employed over the past two decades to study hemodynamics in cerebral aneurysms (Bazilevs *et al.*, 2010). The application of this methodology is justified due to the difficulty of obtaining in vivo measurements of physical flow parameters and the great advancement of imaging diagnostic techniques, which ensure complete mapping of the geometry of a patient-specific cerebral aneurysm through the advent of rotational angiography with three-dimensional reconstruction. Thus, it becomes possible to obtain velocity and pressure fields through computational simulation of blood flow in the patient-specific aneurysm, in order to determine the wall shear stress field and its temporal oscillations on the inner surfaces of arteries and aneurysms – these being the most important parameters for aneurysm initiation, growth, and rupture (Shojima *et al.*, 2004). In this context, the aim of this work is to identify the mechanisms producing the high values of OSI in a patient-specific aneurysm by analyzing the velocity field along the cardiac cycle.

2. METHODOLOGY

2.1 Geometry extraction

The aneurysm analyzed in this study consists of a rare type of posterior circulation IA located at the junction of the basilar artery (BA) with the origin of the left superior cerebellar artery (SCA), as shown in Fig. 1. Geometry was obtained from patient-specific results of an angiography examination. The simulation domain was then extracted using the open-source software known as Vascular Modeling Toolkit (VMTK®) using the marching cubes algorithm. The surface model corresponding to the arterial lumen was then smoothed and clipped to impose boundary conditions.

2.2 Physical modeling

The blood flow was modeled as isothermal and incompressible, and the vessel walls were assumed rigid. Due to the pulsatile nature of cardiac cycle, the flow is unsteady. Moreover, a Newtonian model approximation can be assumed, because the strain rate levels typically found in IAs are higher than 100 s^{-1} (Valencia *et al.*, 2005), which become the non-linear effects of a non-Newtonian model negligible. Due to the small Reynolds numbers along the cardiac cycle, the case can also be modeled as a laminar regime.

The governing equations of flow in integral form for a control volume of surface *S* and volume *V* are the continuity and the momentum equation expressed by the Eq. (1) and (2), respectively.

$$\oint_S \rho \mathbf{v} \cdot \mathbf{n}\, dS = 0, \tag{1}$$

$$\frac{\partial}{\partial t}\int_V \rho \mathbf{v} dV + \oint_S \mathbf{v}\rho\mathbf{v} \cdot \mathbf{n}\, dS = -\oint_S p\mathbf{n}\, dS + \oint_S \mu \nabla \mathbf{v} \cdot \mathbf{n}\, dS, \tag{2}$$

where $\mathbf{v}$ and p are the velocity and pressure fields, n is the unit normal vector pointing outward to the area S, and ρ and μ are the blood density and dynamic viscosity, respectively, equal to 1000 kg/m^3 and 3.3×10^{-3} Pa·s (Isaksen *et al.*, 2008).

Regarding the boundary conditions, at the inlet a parabolic velocity profile for a fully-developed laminar flow in a

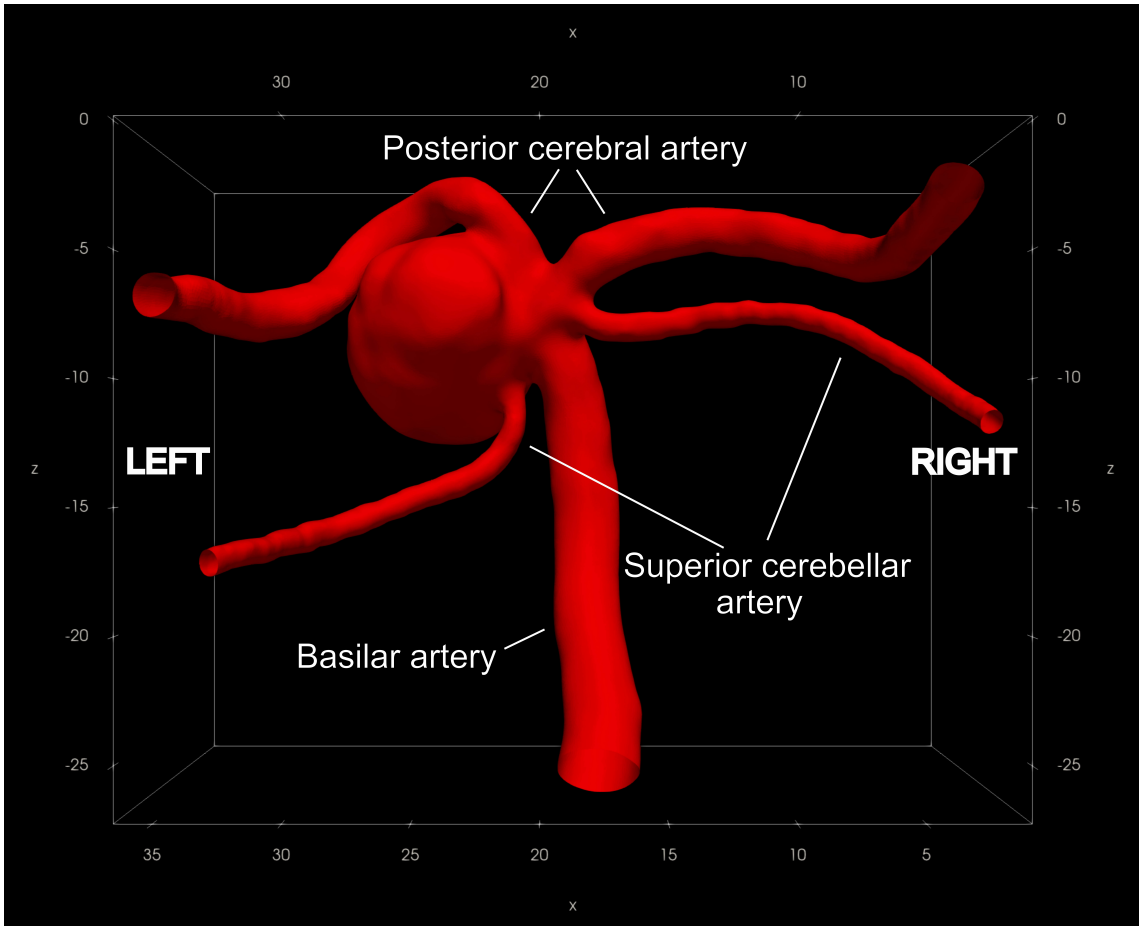

Figure 1. Aneurysm geometry representation with the identification of the vessels (axes grid with units in mm)

pipe, applied along the inward normal vector, was used for the spatial velocity distribution:

$$v_{inlet}(r,t) = 2\frac{q_a(t)}{A_{inlet}}\left[1 - \frac{4r^2}{d_{pa}^2}\right], \tag{3}$$

where $q_a(t)$ is the blood flow rate, A_{inlet} is the cross-sectional area of the inlet artery, d_{pa} is its diameter and r is the radial coordinate of the circular inlet section.

To impose this inlet flow condition, an artificial circular section extension was added to the original inlet artery section with length equals to twice the diameter d_{pa}. The flow rate $q_a(t)$ of the blood pulsatile flow, corresponding to one cardiac cycle, was obtained multiplying the normalized flow rate reported by Hoi *et al.* (2010), for older adults, by the mean flow rate in the basilar artery reported by Zarrinkoob *et al.* (2015). The flow rate profile can be seen in Fig. 2a. Moreover, a zero-gradient pressure condition was adopted in the artery inlet.

In the vessel walls, we adopted a zero-gradient pressure condition and no-slip condition for velocity. At the outlets was imposed a flux corrected velocity with a resistance boundary condition for pressure. This resistance condition is defined by the application of a pressure profile in the outlets proportional to the flow rate profile adopted at the inlet. As can be seen in Fig. 2a, this pressure profile was adopted respecting the threshold values of pressure in a normal cardiac cycle, corresponding to 80 mmHg to the diastole and 120 mmHg to the systole, approximately 11 to 16 kPa. A summary of the boundary conditions applied to the case can be seen in Fig. 2b.

2.3 Numerical solution

Equations (1) to (3) were solved in the computational domain obtained from the geometry extracted from the angiography examination of a patient-specific. The geometry was extracted by the software VMTK® and an OpenFOAM's utility named *snappyHexMesh* was used to obtain a hexahedral dominant mesh. Near to the vessel walls, the cells are general polyhedral with a prismatic boundary layer refinement composed of five layers, as recommended by Oliveira (2022).

The continuity and momentum equations are solved in OpenFOAM by the Finite Volume Method (FVM), which is used to discretize the equations and boundary conditions. In this way, the PISO algorithm (Issa, 1986) was used to solve

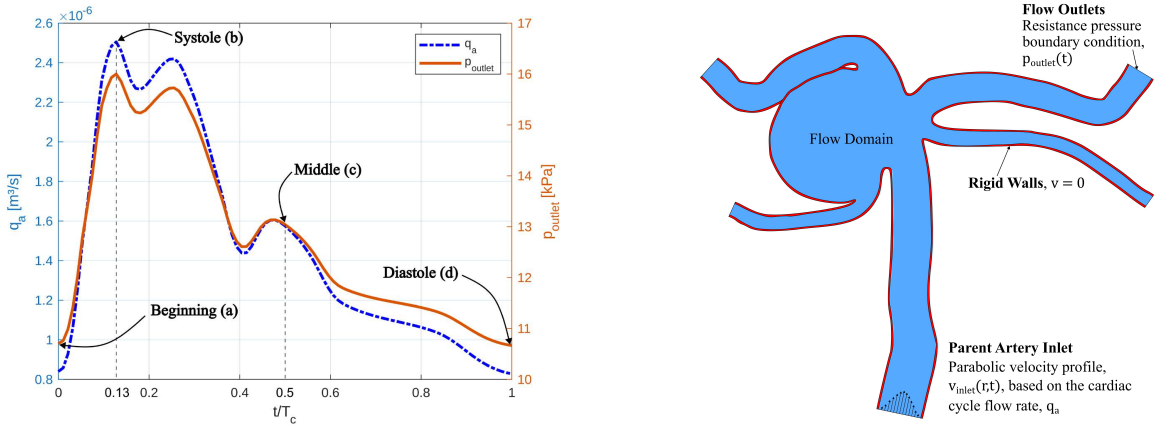

(a) (b)

Figure 2. (a) Flow rate profile used for the parabolic velocity profile in the artery inlet and pressure profile imposed in the outlets by the resistance boundary condition (nondimensional time axis by dividing per the cardiac period, T_c = 0.94 s) and (b) schematic 2D representation with the boundary conditions applied

the pressure-velocity coupling. Regarding the discretization and interpolation schemes, only second-order interpolation profiles were selected to maintain the second-order accuracy level of the FVM. For the advective term of both momentum and pressure equations was used the second-order upwind scheme, with the Green-Gauss scheme for both velocity and pressure gradients discretizations, and the second-order central differences for the surface-normal gradient in the diffusion terms. Moreover, the backward scheme was used to temporal discretization.

An important variable analyzed in this research is the oscillatory shear index (OSI), which indicates how the wall shear stress (WSS) vector varies over the cardiac cycle. OSI can be defined as shown in Eq. (4).

$$OSI(x) = \frac{1}{2}\left(1 - \frac{\left\|\frac{1}{T_c}\int_0^{T_c} \boldsymbol{\tau}_w(\mathbf{x},t)dt\right\|}{\frac{1}{T_c}\int_0^{T_c} \|\boldsymbol{\tau}_w(\mathbf{x},t)\|dt}\right), \tag{4}$$

where T_c is the cardiac cycle period and $\boldsymbol{\tau}$ is the WSS vector. Analyzing the Eq. (4) can be noted that the OSI varies between 0 and 0.5.

3. RESULTS AND DISCUSSIONS

To better understand the origin of high OSI regions on the aneurysm surface, Paraview® was used to visualize the WSS field along the cardiac cycle. The surface limiting streamlines of the flow field in the frontal view of the aneurysm geometry are shown in Fig. 3 superimposed with the OSI fields. These streamlines follow the WSS vector field over the surface and are an approximation of the near-wall flow field (Ardakani *et al.*, 2019). A representation mode named surface LIC (Line Integral Convolution) was applied to the aneurysm surface, which allows visualization of the direction pattern of the WSS field over the OSI field. Figure 3 shows this visualization on the aneurysm surface, revealing the high OSI area over the aneurysm sac. As shown in Fig. 2, we selected 4 time steps to reveal the variation of the WSS vector over the cardiac cycle period: the first one is the beginning of the cycle (t = 0 s), the second one is the peak systole (t/T_c = 0.13), the third one is the middle of the period (t/T_c = 0.5) and the last is the low-diastole instant, corresponding in this case to the end of the cycle (t/T_c = 1). These time steps are represented, respectively, by the letters (a) to (d) in Fig. 3 and 5 in the frontal and posterior view of the geometry of the aneurysm, respectively.

These figures present three vectors on the points identified by the letters A, B and C, which represent the WSS vector at these points. The point A was selected in the high OSI area on the aneurysm sac surface, while points B and C were selected in the low OSI areas on the aneurysm sac and the vessel wall, respectively. This representation is very useful to show the correspondence between the high OSI regions and the high temporal variation of the WSS field lines locally, which is exactly the meaning of the parameter OSI. Another important visualization that helps to justify the appearance of high OSI regions on the aneurysm surface are the streamlines of the velocity field, which are shown in Fig. 4 and 6 from the same viewpoint as the geometry and the same time-steps as those presented in the Fig. 3 and 5, respectively.

Figures 4 and 6 show the origin of the high OSI values inside the aneurysm sac, that is, the circulation of the fluid. The physical mechanism producing this circulation is the shear layer instability at the sac opening. As the main flow encounters the sac's leading edge, the boundary layer that is developed along the artery wall abruptly separates due to the fluid's inertia and the sudden change in geometry. This separated layer transforms into a free shear layer, characterized

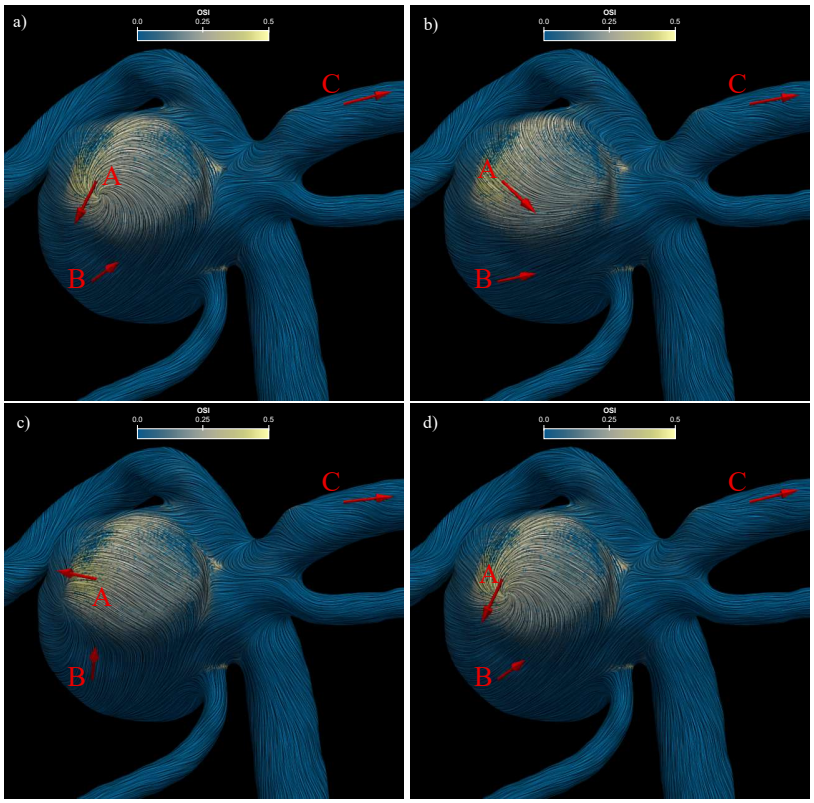

Figure 3. Frontal view of the aneurysm geometry showing the direction pattern of WSS vector represented over the OSI field at the (a) beginning of the cycle, (b) the peak systole, (c) the middle of the period, and (d) the diastole instant

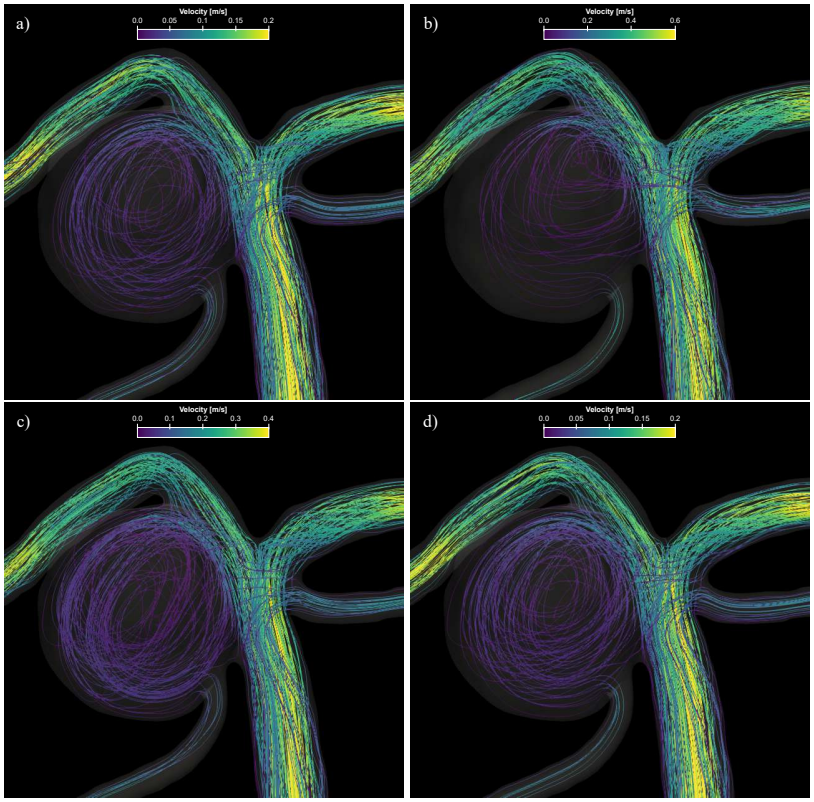

Figure 4. Frontal view of the aneurysm geometry showing the streamlines observed at the (a) beginning of the cycle, (b) the peak systole, (c) the middle of the period, and (d) the diastole instant

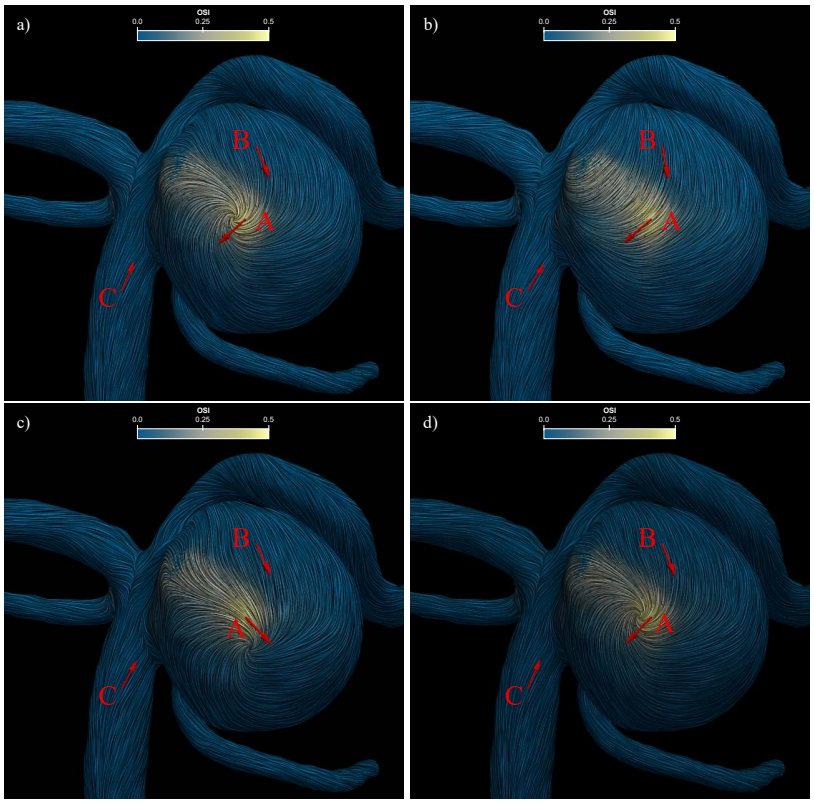

Figure 5. Posterior view of the aneurysm geometry showing the direction pattern of WSS vector represented over the OSI field at the (a) beginning of the cycle, (b) the peak systole, (c) the middle of the period, and (d) the diastole instant

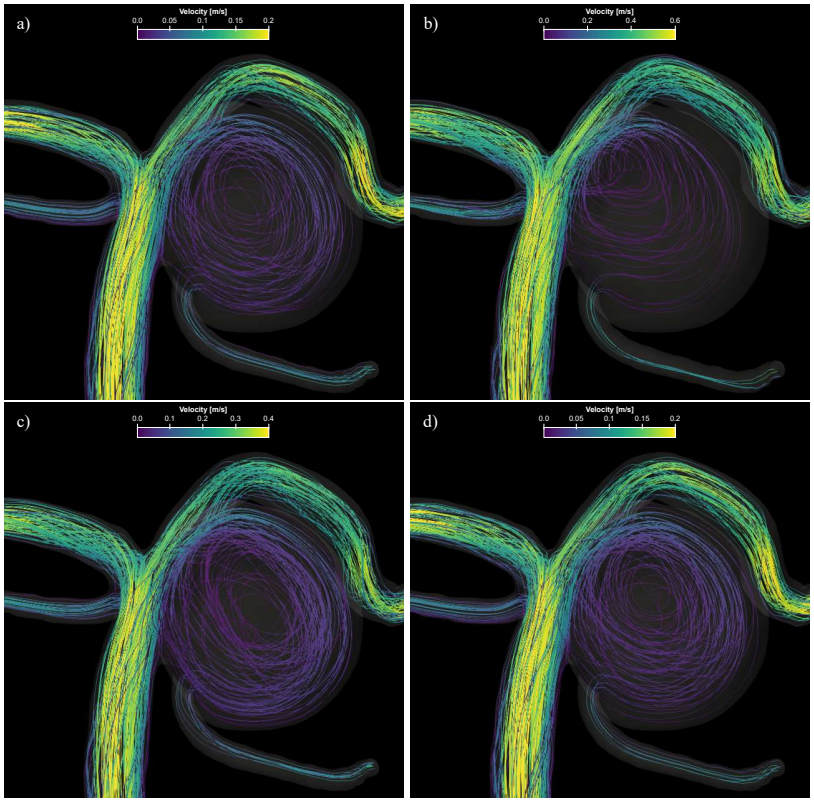

Figure 6. Posterior view of the aneurysm geometry showing the streamlines observed at the (a) beginning of the cycle, (b) the peak systole, (c) the middle of the period, and (d) the diastole instant

by a steep velocity gradient between the faster main flow and the relatively slower (or initially stagnant) fluid inside the sac. This moving viscous shear layer drags the flow inside the aneurysm sac, acting like an invisible "moving lid" over the sac's opening. This combined effect of shearing and dragging induces a large recirculation vortex within the sac. This vortex occupies most of the sac's volume, causing the fluid within it to circulate in the opposite direction to the main flow at the interface with the shear layer, completing its internal rotation. This phenomenon is conceptually analogous to the classic Lid-Driven Cavity Flow problem, where a solid moving boundary induces fluid circulation in a closed cavity.

4. CONCLUSIONS

This research shows that the high OSI values inside the aneurysm sac are caused by the circulation of the flow induced by the shear layer instability at the aneurysm sac opening, a phenomenon conceptually analogous to the classic Lid-Driven Cavity Flow problem, where a solid moving boundary induces fluid circulation in a closed cavity.

5. ACKNOWLEDGEMENTS

This research was supported by resources provided by the Department of Mechanical Engineering of the São Paulo State University (UNESP), School of Engineering, Ilha Solteira, and computational resources supplied by the Center for Scientific Computing (NCC/GridUNESP) of the São Paulo State University (UNESP) and by the National Laboratory of Scientific Computing through the use of the SDumont supercomputer. We thank Hospital Beneficência Portuguesa of São Paulo for providing the case of the study.

6. REFERENCES

Appanaboyina, S., Mut, F., Löhner, R., Putman, C. and Cebral, J., 2009. "Simulation of intracranial aneurysm stenting: Techniques and challenges". *Comput. Methods Appl. Mech. Engrg.*, Vol. 198, pp. 3567–3582.

Ardakani, V.G., Tu, X., Gambaruto, A.M., Velho, I., Tiago, J., Sequeira, A. and Pereira, R., 2019. "Near-wall flow in cerebral aneurysms". *Fluids*, Vol. 4, pp. 1–27.

Bazilevs, Y., Hsu, M.C., Zhang, Y., Wang, W., Liang, X., Kvamsdal, T., Brekken, R. and Isaksen, J.G., 2010. "A fully-coupled fluid-structure interaction simulation of cerebral aneurysms". *Computational Mechanics*, Vol. 46, pp. 3–16.

Etminan, N., Chang, H.S., Hackenberg, K., Rooij, N.K., Vergouwen, M.D.I., Rinkel, G.J.E. and Algra, A., 2019. "World-wide incidence of aneurysmal subarachnoid hemorrhage according to region, time period, blood pressure, and smoking prevalence in the population: A systematic review and meta-analysis". *JAMA Neurology*, Vol. 76, pp. 588–597.

Hoi, Y., Wasserman, B., Xie, Y., Najjar, S.S., Ferruci, L., Lakatta, E.G., Gerstenblith, G. and Steinman, D.A., 2010. "Characterization of volumetric flow rate waveforms at the carotid bifurcations of older adults". *Physiological Measurement*, Vol. 31, pp. 291–302.

Isaksen, J.G., Bazilevs, Y., Kvamsdal, T., Zhang, Y., Kaspersen, J.H., Waterloo, K., Romner, B. and Ingebrigtsen, T., 2008. "Characterization of volumetric flow rate waveforms at the carotid bifurcations of older adults". *Stroke*, Vol. 39, pp. 3172–3178.

Issa, R.I., 1986. "Solution of the implicitly discretised fluid flow equations by operator-splitting". *Journal of Computational Physics*, Vol. 62, pp. 40–65.

Kim, M., Levy, E.I., Meng, H. and Hopkins, L.N., 2007. "Quantification of hemodynamic changes induced by virtual placement of multiple stents across a wide-necked basilar trunk aneurysm". *Neurosurgery*, Vol. 61, pp. 1305–1313.

Meng, H., Tutino, V.M., Xiang, J. and Siddiqui, A., 2014. "High wss or low wss? complex interactions of hemodynamics with intracranial aneurysm initiation, growth, and rupture: Toward a unifying hypothesis". *AJNR*, Vol. 35, pp. 1254–1262.

Oliveira, I.L., 2022. *On the mechanics of intracranial aneurysms walls: Numerical assessment of the influence of tissue hyperelastic laws and heterogeneity and the major role played by curvature on pathways to rupture*. Ph.D. thesis, São Paulo State University, Ilha Solteira, Brazil.

Sforza, D.M., Putman, C.M. and Cebral, J.R., 2009. "Hemodynamics of cerebral aneurysms". *Annu Rev Fluid Mech*, Vol. 41, pp. 91–107.

Shojima, M., Oshima, M., Takagi, K., Torii, R., Hayakawa, M. and Katada, K., 2004. "Magnitude and role of wall shear stress on cerebral aneurysm". *Stroke*, Vol. 35, pp. 2500–2505.

Tsianaka, E., Al-Shawish, A., Potapov, A., Fountas, K., Spyrou, M. and Konovalov, N., 2019. "Magnitude and role of wall shear stress on cerebral aneurysm". *Chinese Neurosurgical Journal*, Vol. 5, pp. 1–12.

Valencia, A.A., Zárate, A., Gálvez, M. and Badilla, L., 2005. "Non-newtonian blood flow dynamics in a right internal carotid artery with a saccular aneurysm". *International Journal of Numerical Methods in Fluids*, Vol. 50, pp. 751–764.

Van Gijn, J., Kerr, R. and Rinkel, G., 2007. "Subarachnoid haemorrhage". *Lancet*, Vol. 369, pp. 306–318.

Van Gijn, J. and Rinkel, G., 2001. "Subarachnoid haemorrhage: diagnosis, causes and management". *Brain*, Vol. 124, pp. 249–278.

Vlak, M.H.M., Algra, A., Brandenburg, R. and Rinkel, G.J.E., 2011. "Prevalence of unruptured intracranial aneurysms, with emphasis on sex, age, comorbidity, country, and time period: a systematic review and meta-analysis". *Lancet Neurol*, Vol. 10, pp. 626–636.

Zarrinkoob, L., Ambarki, K., Wåhlin, A., Birgander, R., Eklund, A. and Malm, J., 2015. "Blood flow distribution in cerebral arteries". *Journal of Cerebral Blood Flow and Metabolism*, Vol. 35, pp. 648–654.

7. RESPONSIBILITY NOTICE

The authors are solely responsible for the printed material included in this paper.